Fabrication of a luminescent solar concentrator that minimizes self-absorption losses using inter-chromophore energy transfer

by

Michael James Currie

Submitted to the Department of Electrical Engineering and Computer Science
in partial fulfillment of the requirements for the degree of

Master of Science in Electrical Engineering and Computer Science

at the

MASSACHUSETTS INSTITUTE OF TECHNOLOGY

June 2007

Author .....
Department of Electrical Engineering and Computer Science
June 2007

Certified by.....
Marc A. Baldo
Esther and Harold Edgerton Assistant Professor of Electrical Engineering and Computer Science
Thesis Supervisor

Accepted by .....
Arthur C. Smith
Chairman, Department Committee on Graduate Theses
Electrical Engineering and Computer Science

Fabrication of a luminescent solar concentrator that minimizes self-absorption losses using inter-chromophore energy transfer

by

Michael James Currie

Submitted to the Department of Electrical Engineering and Computer Science
on June 2007, in partial fulfillment of the
requirements for the degree of
Master of Science in Electrical Engineering and Computer Science

Abstract

The projected need for carbon-free power during this century is immense. Solar power offers the largest resource base to supply this need, but in light of recent silicon shortages, it is an open question whether silicon photovoltaics can keep pace with demand. The development of economical concentrators could relieve this resource pressure. The luminescent solar concentrator (LSC) is an architecture that collects and concentrates light using the luminescent properties of chromophores embedded in a waveguide. This method of concentration alleviates the need for expensive tracking equipment necessary for optical concentration. Combined with the low cost and flexible fabrication of organic materials, this technology is inherently scalable.

A major limitation to LSC efficiency is self-absorption between different chromophores within the waveguide. Finding inspiration from the architecture of phycobilisome antenna complexes, a system of chromophores is developed that minimizes self-absoprtion through Förster energy transfer. Precise control of intermolecular spacing is achieved through thermal evaporation of small molecule organics. A LSC with a geometric gain of 25 is fabricated that employs this optimized system. External quantum efficiencies of 32% are achieved across nearly half the visible spectrum, with a total power conversion efficiency of 1.6%. Additionally, modeling and theory are presented to highlight places for device improvement. It is shown that a simple path integral successfully captures the dynamics of the LSC.

Thesis Supervisor: Marc A. Baldo
Title: Esther and Harold Edgerton Assistant Professor of Electrical Engineering and Computer Science

Acknowledgments

I owe much thanks and appreciation to Marc Baldo, my supervisor, for allowing me to follow my gut and for providing an atmosphere to tackle the critical problems, not just the *en vogue* problems.

The Soft Semiconductor Group has offered invaluable advice and support, specially Tim Heidel – with whom debugging fabrication and test equipment is always a joy, for offering engineering solutions for the sake of my time and sanity and helping me survive my first year; Jon Mapel – who shares my sustainable passions and who *truly* taught me scientific experimentation; Kaveh Milaninia – for always offering dead-on tactical advice; Michael Segal – for getting me off the ground with organic theory; and, Carlijn Mulder – for exceptional experimental assistance and contagious enthusiasm first thing in the morning, errr, just after coffee.

To my wife, life partner and expectant mother of our child, Aiyana – I begin and end each day in your arms. You are my inspiration, best friend and wellspring who replenishes my spirit. Thank you for supporting every moment of our lives.

This thesis is dedicated in the loving memory of my mother, Patricia. For the past two years, she has kept constant watch over me in the lab. Thank you mom for your unshakable love and belief in me. It's about time, right?

Contents

1 Introduction **13**

1.1 Motivation 13

1.2 Energy Trends and Carbon Emissions 13

1.3 Current status of Photovoltaics 14

1.4 Role for Organic Photovoltaics 16

1.5 Argument for an Organic Concentrator 17

2 Luminescent Solar Concentrator Operation and Theory **19**

2.1 LSC Description and Coordinate System 19

2.2 Trivial Efficiency Model 20

2.3 Developed Efficiency Model 24

2.3.1 Origin of Self-Absorption and Stoke's Shift 24

2.3.2 Role of Self-Absorption 25

3 Numerical Models to Predict Self-Absorption **31**

3.1 Self-Absorption Path Integral 31

3.2 Two Dimensional Numeric LSC model 35

4 Pathway to an Efficient LSC **39**

4.1 Historical Implementations 39

4.2 Material Stability Improvements 41

4.3 Strategy to Minimize Self-absorption 42

5 LSC Fabrication and Testing **45**

5.1 LSC Fabrication 45

5.1.1 Optimized Thin Film 45

5.1.2 Choice of Substrate 48

5.1.3 Choice of Photovoltaic 49

5.1.4 Fabrication Steps of Optimized LSC 50

5.1.5 Measured Absorption Constants and EQE Measurement . . . 51

6 Conclusion **55**

List of Figures

2-1 Schematic of an LSC 21

2-2 Total Power Conversion Limits for an LSC 23

2-3 Radiative Transitions in Molecules 24

2-4 Photon Flow Diagram 27

3-1 Absorption and photoluminescence Spectra for neat rubrene 32

3-2 Average Self-absoprtion versus geometric gain 34

3-3 2D Path Integral Map 36

4-1 Phycobilisome structure and Spectra 43

5-1 PL Spectra of Alq_3:DCJTB(x%) 46

5-2 PL Spectra of Alq_3:Rubrene(40%):DCJTB(x%) 47

5-3 PL Spectra of Alq_3:Rubrene(40%):DCJTB(x%) 48

5-4 EQE spectrum of single and multi crystalline solar cells 50

5-5 Absorption and PL spectrum of Alq_3:Rubrene(45%):DCJTB(2.5%) . 52

5-6 Optimized LSC External Quantum Efficiency 53

List of Tables

3.1 Self-absorption for common OLED materials 33

5.1 η_{TPCE} for optimized LSC 53

Chapter 1

Introduction

1.1 Motivation

Ultimately, this thesis details the science, research and fabrication of a type photovoltaic device, capable of converting sunlight into electrical power. Initially, however, this work is inspired and shaped by trends in energy use, climate impact, economics and lesson learned in the burgeoning field of organic electronics. A mature power conversion device must successfully address these issues, or else, it will not survive the scrutiny of the marketplace. For the researcher, a fledgling power conversion device must show the potential, under reasonable assumptions, to address these issues. With that mandate in mind, this thesis investigates the potential of the luminescent solar concentrator (LSC).

1.2 Energy Trends and Carbon Emissions

Historically, standards of living among humans are linked to the availability of energy. In 2000, the per capita consumption of primary energy of North America was 280 gigajoules (GJ) and the Organisation for Economic Co-operation and Development (OECD) nations of Europe and the Pacific consumed 142 and 180 GJ. This is in stark contrast to sub-Saharan Africa, China and Asia which used 25, 38 and 28 GJ per capita respectively.[1] Increased standards of living in these developing nations

will be accompanied by higher per capita primary energy consumption. In addition, any population gains will also add energy demand. Indeed, over the past decade the growth rate in primary energy usage in the developing world is twice (3.19% versus 1.52%) than that of the OECD nations.[1]

Fossil fuels comprise 80% of primary energy production.[1] Unless the increased consumption is derived from carbon-free renewable energy sources, we can expect the amount of carbon dioxide (CO_2) released per annum to increase. The amount of CO_2 released per annum during energy production is given by the Kaya identity.[2]

$$\dot{M} = N * GDP/N * \dot{E}/GDP * C/E$$

Here, N is the global population, GDP/N is the per capita gross domestic product, $\dot{E}/GDP$ is the primary energy intensity and C/E is the carbon intensity. Using data from the previous century, the Intergovernmental Panel on Climatc Change has forecast these four factors out to the year 2100 under different scenarios. The baseline scenario includes no alteration to climate change policy and has been used as a benchmark. Built into this scenario is the assumption that carbon intensity decreases at a rate of 1% per year, but still carbon emissions will increase from 6 gigatons of carbon per year to 20 gigatons of carbon per year in 2100. To meet the global power demand and continue on the carbon intensity curve of the baseline scenario, it is calculated that we will need to create 10 terawatts (TW) of carbon-free power by 2050. In order to stabilize carbon levels at twice the pre-industrial level (550 parts per million) the 10 TW must be brought online by 2035.[3] By comparison in 1990, global primary energy consumption was 11 TW. A truly extraordinary amount of carbon-free power must be brought online over the course of the next century to preclude significant changing of our climate system.

1.3 Current status of Photovoltaics

The incumbent photovoltaic technology is the single junction silicon solar cell. A large degree of its success is due to the development of high-quality silicon processing

technologies of the microelectronics industry. These have driven historic improvements in cost and power conversion efficiencies. Typical values for power conversion efficiency for a silicon photovoltaic module range from 8.2% to 22.7%, depending on the crystallinity of the base silicon solar cell[4], with the average module efficiency of 12.5%.[5] The highest recorded efficiency for a single junction silicon cell is 24.7%. To achieve this level, extremely pure silicon in conjunction with sophisticated light trapping is employed.[6]

In stride with efficiency improvements, the annual production of silicon photovoltaics has been rising at 30% per year.[5] More recently, the industry produced 2.54 gigawatts (GW) of solar cells in 2006. This compares to 1.81 GW and 1.26 MW in 2005 and 2004, respectively. The last two years have seen growth at over 40%.[7] With this heady growth has come a silicon shortage that is attracting huge amounts of capital.

The cost of silicon photovoltaic power traditionally follows an industry learning curve. For every doubling of production, the cost per watt falls 20%.[5] The period between 2004 and 2006 represents a production doubling. However, the retail price per watt for a 125 W module has increased from $4.32 in May 2004 to $4.86 in May 2006.[8] If the silicon shortage is relieved, the learning is expected to continue.

At what rate would silicon photovoltaic production need to increase to achieve 10 TW of carbon-free power by 2050? Since the sun only shines during half the day, a larger installed base of photovoltaics would be required. Assuming six peak hours per day, equivalent to 40 TW operating at 25% capacity, the growth rate would need to be 20.1% per year for the next 43 years. This is a doubling every 3 to 4 years. In the year 2050, we would need to produce 6.7 TW of new solar power. Allowing a modest efficiency gain to 20%, this will cover an area of 33,000 square kilometers, roughly the combined area of Connecticut and Massachusetts. This is truly a huge number, and photovoltaics can only be a portion of the solution.

1.4 Role for Organic Photovoltaics

Because of shear size and economics of the problem, organic photovoltaics has received considerable attention. Organic materials are typically inexpensive when produced in industrial quantities and are compatible with multiple fabrication techniques and substrates.[9] The holy grail of organic photovoltaics is an efficient cell able to be mass-produced using roll-to-roll processing, much like newsprint.

Intense research into organic solar cells has progressed since the first bi-layer heterojunction cell introduced by Tang in 1986. A recent tandem organic solar cell was reported to have a 5.7% power conversion efficiency.[10] This is five times smaller than inorganic multi-junction cells, which regularly exceed 30% efficiency. Additionally, the organic cells have not achieved large area. Most devices are much smaller than 1 cm^2.

The technical challenge in organic solar cells is the balance between absorption and charge separation. To efficiently separate an exciton (molecular excited state) into an electron and hole requires that the exciton be formed on the order of one diffusion length, typically 10 nm, from the separating junction. Otherwise the exciton will have a high probability of relaxing back to the ground state. Unfortunately, the absorption lengths in organics are typically longer than 100 nm. To satisfy both requirements, researchers have focused on creating thicker, bulk devices where the separating junction is three-dimensional, thus providing a nearby surface throughout.

The dominant feature of organic molecules is their strong tendency to interact with light and create excited states. The excited state can relax to the ground state by coupling to vibrational modes of the molecule or by radiatively relaxing through photon emission, both of which shorten the diffusion distance. The second relaxation pathway, radiative recombination, gives these molecules strong optical properties. The laser dye industry and the emerging organic light emitting display (OLED) industry take advantage of these optical properties.[11]

1.5 Argument for an Organic Concentrator

Why concentrate? If you can provide more irradiance through concentration for less cost than increasing the amount of solar cell to achieve the same level of irradiance, it makes sense to concentrate. The economics of concentration are specially valid in the face of supply demand, as is the case for silicon. Additionally, if concentration is inexpensive, it is beneficial to use the highest efficiency cell material possible.

Conventional light concentration uses optics to focus light onto a solar cell. For optimum performance, the focal point of the light must be maintained as the sun transits the sky. The system relies on tracking equipment to keep this focal point. Such mechanical systems are expensive to maintain and deploy. Also they require extra spacing to avoid shadowing neighboring concentrators. The simplicity of the flat solar panel is lost.

As mentioned previously organic materials are inexpensive and can be easily fabricated. In addition, they have strong optical properties, in terms of absorption and re-emission of light. A concentrator could be achieved by absorbing light over a large area and re-directing the emission of light to a high efficiency solar cell. This device would not need tracking equipment. Such a device, known as the luminescent solar concentrator (LSC) was proposed in the late 1970's.[12] At that time, the concept was explored using laser dyes as the organic material. The technical barrier to widespread adoption was degradation of the laser dye.[13] The OLED industry has largely solved the degradation problem through chemical synthesis and encapsulation of its organic materials. Typical reported lifetimes are 20,000 to 100,000 hours. The LSC stands to directly benefit.

Chapter 2, of this thesis will detail of the operation and efficiency calculations of an LSC. The chapter closely follows the previous work of Batchelder. Two numerical models for LSC design and performance are presented in Chapter 3. Chapter 4 provides a brief overview of other work in the field and discusses how energy transfer between organic molecules can be used to enhance performance. A model from nature is proposed as an ideal system system, and a synthetic analog is suggested to emulate

this system. Chapter 5 covers the fabrication and testing of an optimized organic solid state LSC. And, chapter 6 concludes by summarizing this work and addressing the next steps in LSC research.

Chapter 2

Luminescent Solar Concentrator Operation and Theory

2.1 LSC Description and Coordinate System

Generically, the LSC is a device that absorbs light by a system of one or many chromophores and redirects, or waveguides, the luminscent emission the chromophore system toward a transducer. The transducer can be any device that takes advantage of the light. In this work, I will consider the use of a photovoltaic for electrical conversion, although other uses such as daylighting have been suggested.[14] The simplest manifestation of an LSC is a glass (or plastic) substrate embedded with single or multiple chromophores, or dyes. This is the geometry that is explored in this thesis. Upon absorption of incident light, the dye(s) luminesces isotropically. Due to the total internal reflection provided by the air/glass/air interface, a fraction of the light is trapped inside the glass. A photovoltaic (PV) appropriately attached to the edge of the glass sheet collects this trapped light. By ensuring the area of the glass sheet is larger than the PV, a geometric concentration factor is achieved. Formally it is given by:

$$G_{geo} = A_{sheet}/A_{photovoltaic} \tag{2.1}$$

For a square LSC, G_{geo} is trivially L/D where L is the length of the sheet and D

is the thickness of the sheet. A rectangular LSC is illustrated in Figure 2-1. The coordinate system of the LSC is designated as follows: The x-axis is normal to the PV in the plane of the substrate. The y-axis is in the plane of both the substrate and PV. The z-axis is normal to the substrate and in the plane of the PV. Angle theta is the angle with respect to the z-axis. Angle phi is the angle in the $x-y$ plane with zero degrees in the y-axis.

2.2 Trivial Efficiency Model

A measure of efficiency for an optical device is the external quantum efficiency (EQE). It is defined as the ratio of the number of electrons produced by the device divided by the total number of photons incident on the device. This metric is appropriate for the LSC since it is an optical device. The EQE is a function of a numerous subcomponents efficiencies. To understand the basic functionality of the LSC, we imagine a trivial LSC that has the following attributes: (1) The substrate is a perfect substrate with an index of refraction n_{sub}. (2) Perfect mirrors are attached to the remaining three faces of the LSC and (3) the LSC contains a single dye with no overlap between its absorption spectrum and emission spectrum. When the dye luminesces, it will not be reabsorbed by other dye molecules in the substrate. The EQE of the device is then given by:

$$\eta_{EQE} = \eta_{abs}\ \eta_{PL}\ \eta_{trap}\ \eta_{PV} \tag{2.2}$$

Here η_{abs} is the fraction of light absorbed by the dye, η_{PL} is the quantum yield of luminescence of the dye. This term combines both emission from singlet and triplet excited states. η_{trap} is the fraction of light trapped within the waveguide as a result of total internal relection at the substrate/air interface. It is given by $\sqrt{1-1/n_{sub}^2}$. The solid angle over which light is trapped is known as the trap cone, and the solid angle over which light escapes is known as the escape cone. η_{PV} is the EQE of the PV coupled to the substrate. All of these factors can be a function of wavelength, λ. For the case of a glass substrate, with $n_{sub} = 1.5$, the maximum EQE is 0.745.

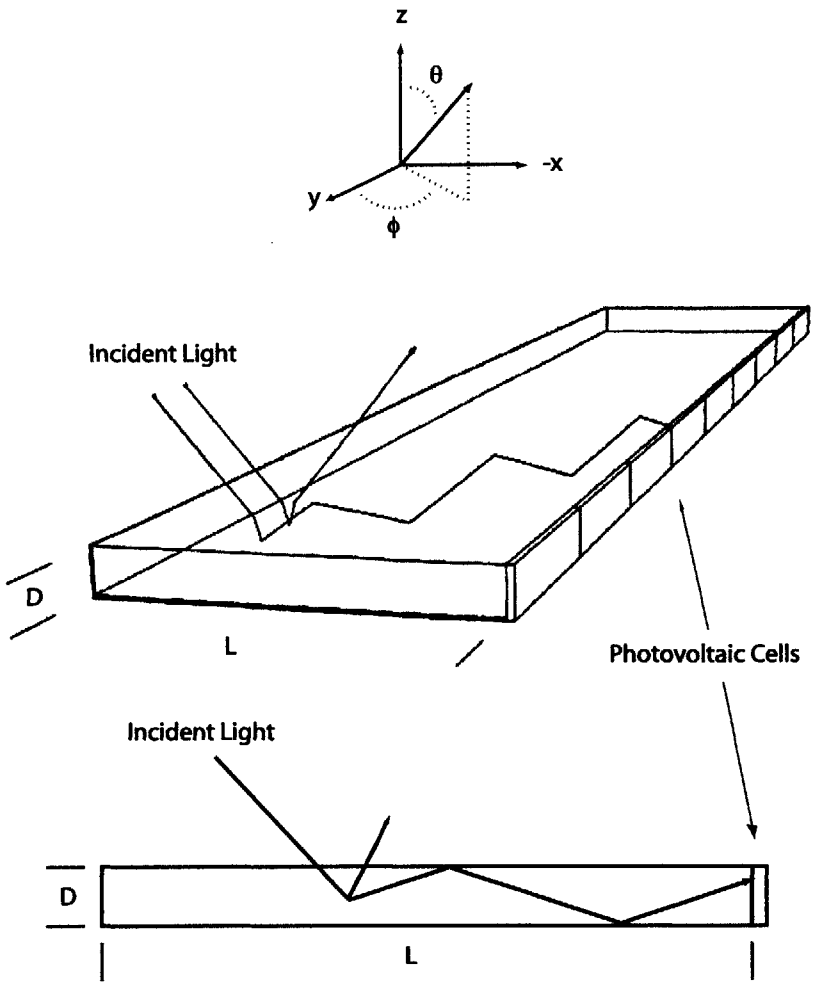

Figure 2-1: **Schematic of an LSC** – The above shows a perspective and cross-sectional view of an LSC. Incident light is absorbed and re-emitted by a chromophore within the LSC. A fraction of the light will be trapped inside the waveguide and the remainder will escape. The coordinate system that will be adhered to throughout this thesis is shown above. Perspective schematic derived from[15]

By knowing the performance of the attached PV, the total power conversion efficiency, η_{TPCE} can be calculated. The power at the optimum operating point of the PV is given by $P_{max} = I_{sc} \times V_{oc} \times FF$ where I_{sc} is the short circuit current, V_{oc} is the open circuit voltage and FF is the fill factor of the cell. Using the EQE computed above we can compute the I_{sc} of the LSC by:

$$I_{sc} = \frac{q\ A_{LSC}}{hc} \int_0^{\frac{hc}{E_g}} \eta_{EQE}(\lambda)\ E(\lambda)\lambda d\lambda \tag{2.3}$$

where $E(\lambda)$ is the incident solar spectral irradiance, h is Planck's constant, c is the speed of light and E_g is the bandgap of the PV. Then, the total power conversion efficiency is expressed as:

$$\eta_{TPCE} = \frac{V_{oc}\ FF\ \frac{q\ A_{LSC}}{hc} \int_0^{\frac{hc}{E_g}} \eta_{EQE}(\lambda)\ E(\lambda)\ \lambda\ d\lambda}{A_{LSC}\ \int_0^{\frac{hc}{E_g}} E(\lambda)\ d\lambda} \tag{2.4}$$

Figure 2-2 shows the cumulative total power conversion efficiency versus wavelength for an ideal LSC, i.e. 100% EQE, and an ideal glass LSC coupled to either a gallium arsenide or silicon PV. The calculation assumes the dye has unity quantum yield, completely absorbs the complete ASTM AM 1.5 Global solar spectrum and has no self-absorption. The fill factors and open circuit voltages are derived from the record crystalline cells.[6] The actual efficiencies will, in practice, be higher due to the logarithmic increase of V_{oc} with increasing photocurrent.

Rarely is the trivial model applicable to an actual luminescent solar concentrator. All dyes have vibrational and rotational states that broaden their electronic energy levels. In addition, the local environment can contribute to further homogeneous broadening. This potentially causes a non-zero overlap between the absorption and emission spectra. A non-zero overlap contributes to self-absorption among dyes, which quickly complicates the model of the LSC.

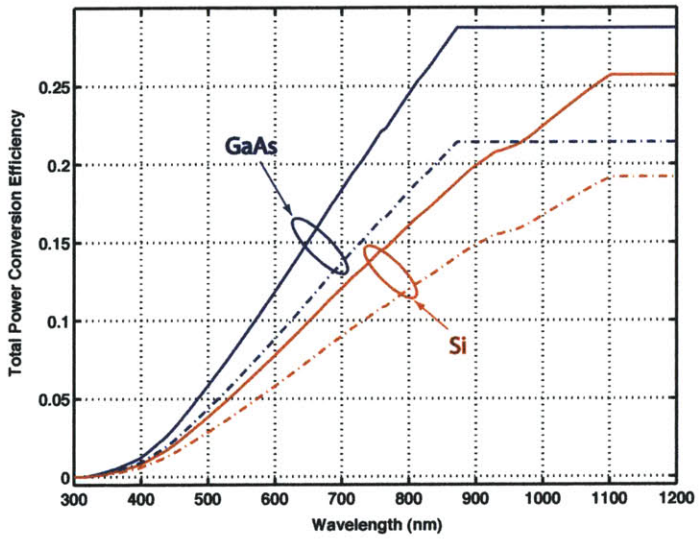

Figure 2-2: **Total Power Conversion Limits for an LSC** – This figure shows the cumulative total power conversion efficiency for an LSC coupled to GaAs and Si solar cells. The solid lines are an ideal system with unity EQE and the dashed lines are an ideal LSC on glass. The dye is assumed to have unity quantum yield, completely absorbs the complete ASTM AM1.5 Global solar spectrum and has no self-absorption.

2.3 Developed Efficiency Model

2.3.1 Origin of Self-Absorption and Stoke's Shift

Molecules are comprised of numerous atoms bonded together. The oscillations and torsions of these bonds between nuclei give rise to vibrionic and rotational states in addition to the electronic states. The difference between two consecutive vibrionic or rotational states is much smaller than the difference between consecutive electronic states. Then each electronic state can be viewed as a manifold of states that include its vibrionic and rotational states. Figure 2-3 shows the energy diagram versus reaction coordinate for the S0 and S1 electronic states of a notional molecule.

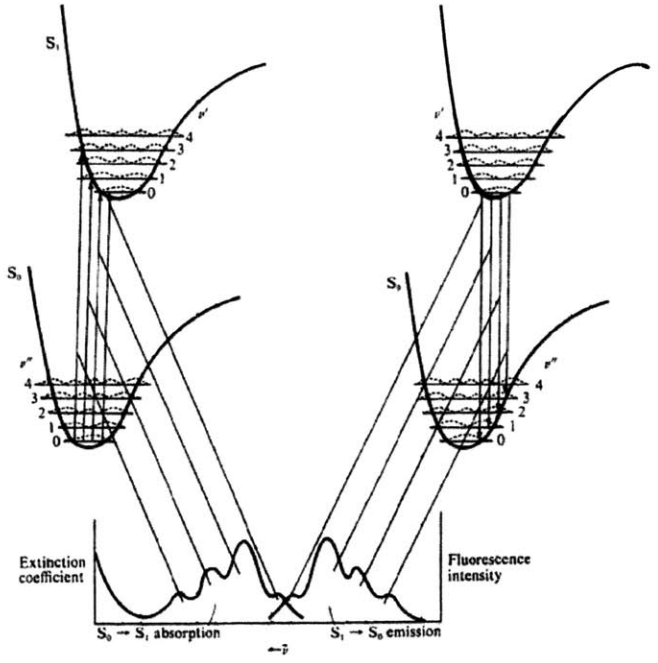

Figure 2-3: **Radiative transitions in molecules** – This figure depicts the radiative transition from the ground state, S0, manifold to the first excited state, S1, manifold. The Frank Condon Principle predicts that the nuclear configurations do not change instantaneously. Thus a transition is most likely between electronic configurations that have the largest spatial overlap. Within the S1 manifold, an excited state falls to the lowest vibrionic state in picoseconds. This relaxation produces a downward shift in energy for the radiative transition back to the S0 manifold. This is known as the Stoke's shift of the molecule. Graphic taken from [16]

Due to the numerous states in each manifold, there are many possible transitions for an electron from a ground state to an excited state. According to the Frank-

Condon principle when a photon is absorbed, the electronic transition happens much quicker than the heavy nuclear framework can react. The probability of a given transition is proportional to the overlap of the ground state and excited state wave-functions. The many transition energies give rise to broadened absorption spectra. After an electron is excited, it immediately falls to the lowest energy level of that electronic manifold. From here, it can radiatively recombine to the numerous ground state levels. The lowering of the energy after absorption and before emission is known as the Stoke's shift of the molecule. Formally, it is calculated as the distance from the peak absorption wavelength to the peak emission wavelength. Additionally, when a molecule is placed in an environment, it can interact with other molecules, as in the case with amorphous thin films and solvation effects in liquids and solids.[17] This interaction causes additional variation in the energy levels. If the total broadening is significant relative to the Stoke's shift, the absorption spectra and emission spectra will exhibit overlap.

2.3.2 Role of Self-Absorption

Because of self-absorption, not all photons that are re-emitted by the dye within the LSC make it to PV. These photons are absorbed by other dye molecules, which in turn re-emit new photons. This process occurs *ad infinitum.* These subsequent excitation/emission events are labeled generations. Subsequent generations' emissions are red-shifted as a result of conservation of energy and slightly reduce the degree to which the next generation is self-absorbed.

To model these effects, following Batchelder, we define two self-absorption probabilities: r, the average probability that a photon emitted in the trap cone is self-absorbed and $\bar{r}$, the probability that a photon emitted in the escape cone is self-absorbed. We also define the probability of a photon being in the escape cone as P, thus the probability of being in the trap conc is $(1 - P)$. Note that $(1 - P)$ is the same value as η_{trap} above. Thus the probability of the first generation reaching the PV, $Q^{(1)}$ is given by:

$$Q^{(1)} = \eta_{PL}(1-r)(1-P) \tag{2.5}$$

and the fraction of re-absorbed light in the first generation, $RA^{(1)}$, is :

$$RA^{(1)} = \eta_{PL}[\bar{r}P + r(1-P)] \tag{2.6}$$

Any subsequent probability $Q^{(i)}$ can be expressed as a recursive relation:

$$Q^{(i)} = [\eta_{PL}(1-r)(1-P)]RA^{(i-1)} \tag{2.7}$$

The total probability Q is the summation of all $Q^{(i)}$. We identify the summation as a converging geometric series.

$$Q = \sum_{i=1}^{\infty}[\eta_{PL}(1-r)(1-P)]\{\eta_{PL}[\bar{r}P+r(1-P)]\}^{i-1} = \frac{\eta_{PL}(1-r)(1-P)}{1-\eta_{PL}[\bar{r}P+r(1-P)]} \tag{2.8}$$

The probability, Q, can be thought of as transport efficiency, η_{trans} which takes into account the recursive influences of photoluminescence, waveguide trapping and self-absorption.

Self-absorption can, also, be modeled as feedback. This is illustrated in the photon flow diagram of Figure 2-4 from Batchelder. The model starts with the solar photon flux from the sun. Immediately, the air/substrate interface reflects a portion of the flux and this flux is lost from the system. Of the non-reflected flux a portion S is absorbed. Unabsorbed photons are also lost. In steady state, the excitation rate, J, is caused by S and the portion of photoluminesced light, $J\ \eta_{PL}$, that is self-absorbed. A fraction of light P, or $1-\eta_{trap}$, will be in the escape cone, while $1-P$, or η_{trap}, will be in the trap cone. Light in these cones are reabsorbed with average probability $\bar{r}$ and r for the escape and trapped cone, respectively. The equation for J is:

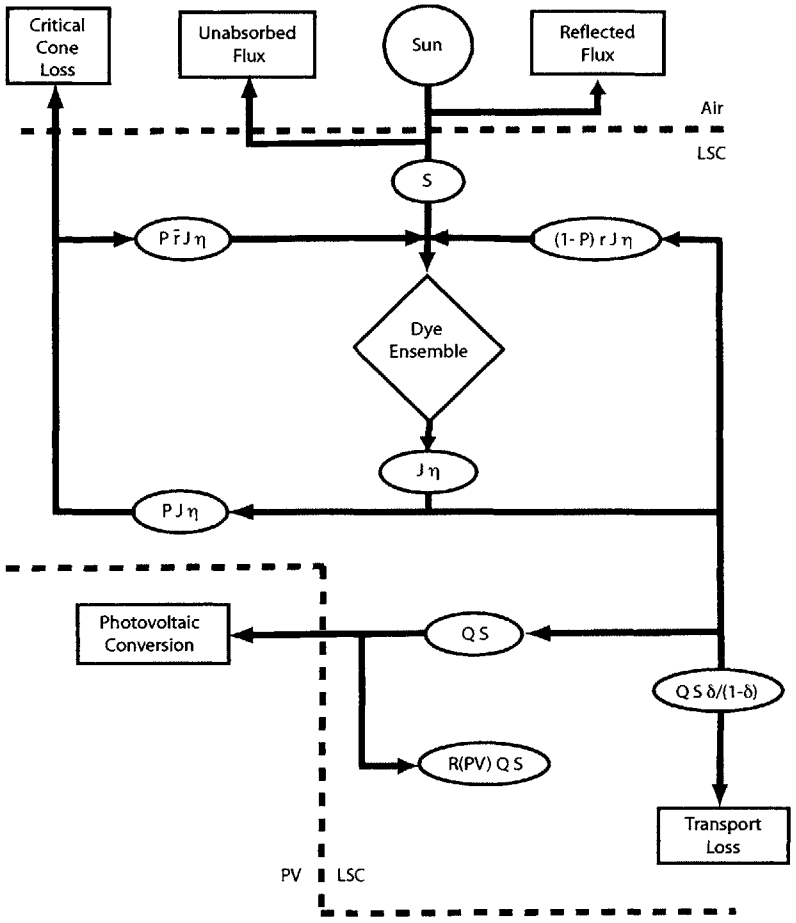

Figure 2-4: **Photon Flow Diagram** – A photon flow diagram depicting the predominant channels available in the LSC. Dotted lines represent changes in index of refraction and squares represent photons sinks. Light from the sun enters the dye ensemble, resulting in luminescence that is converted in the PVC. The two feedback loops around the dye ensemble represent the effects of self-absorption inside and outside the critical cones. Graphic and caption taken from [15]

$$J = SA_{LSC} + J\eta_{PL}r(1-P) + J\eta_{PL}\bar{r}P \tag{2.9}$$

$$J = SA_{LSC}/\{1 - \eta_{PL}[r(1-P) + \bar{r}P]\} \tag{2.10}$$

Knowing J, the total flux, W arriving at the photovoltaic is the fraction of photoluminesced light in the trap cone that reaches the PV. This is given by:

$$W = J\eta_{PL}(1-r)(1-P) \tag{2.11}$$

$$W = SA_{LSC}\eta_{PL}(1-r)(1-P)/\{1 - \eta_{PL}[r(1-P) + \bar{r}P]\} \tag{2.12}$$

$$W = SA_{LSC}Q \tag{2.13}$$

Both methods give the same result. Since $\bar{r}$ plays a small role in a properly designed system, the model is applicable to the extent that r correctly captures the dynamics of self-absorption. For the case of a LSC surrounded on four sides by PV, it is appropriate to estimate r as the self-absorption probability of a dye situated in the center of an LSC plate.

The above analysis predicts the performance for an uniformly illuminated LSC. If the irradiance varies in the x-axis or y-axis, a full numerical simulation of the LSC is required. Light absorbed and re-emitted of a certain wavelength at a point (x, y) will have a unique probability of reaching the PV, and full accounting must take place. This model will be presented in Chapter 3.

An interim summary, at this point, is worthwhile. Revisiting the initial EQE equation, we can adjust and add new terms to give a better prediction of device performance.

$$\eta_{EQE} = \eta_{abs}\eta_{PV}\frac{\eta_{PL}(1-r)(1-P)}{1-\eta_{PL}[\bar{r}P + r(1-P)]} \tag{2.14}$$

$$= \eta_{abs}\eta_{PV}\frac{\eta_{PL}\eta_{trap}(1-r)}{1-\eta_{PL}[(1-\eta_{trap})\bar{r} + \eta_{trap}r]} \tag{2.15}$$

$$= \eta_{abs}\eta_{PV}\eta_{trans} \tag{2.16}$$

The first term constitutes the amount of light absorbed by the dye, including reflections of the solar flux off the LSC. The second term is the EQE of the attached PV. This should be selected for optimum performance. The remaining terms with the exception of the trapping efficiency are properties of the dye. Simply, the dye needs to absorb as much of the solar spectrum as possible, have near unity quantum yield and have minimal overlap. Unfortunately, no single dye can accomplish these tasks simultaneously.

Chapter 3

Numerical Models to Predict Self-Absorption

3.1 Self-Absorption Path Integral

If we know the absorption and emission spectra along with the quantum yield of luminescence of a dye, we are able to model its suitability in an LSC. The intensity, I of electromagnetic wave traveling in an absorptive media is defined by the Beer-Lambert law, $I = I_0 e^{-\alpha(\lambda)Cx}$. Here, $\alpha(\lambda)$ is the molar extinction coefficient in units $M^{-1}cm^{-1}$, C is the molar concentration and x is the path length in centimeters. By applying the Beer's Lambert Law weighted over the dye emission spectrum we can compute the fraction of intensity transmitted a distance x centimeters away. This is integral is given by:

$$fraction = \int_0^\infty f(\lambda) e^{-\alpha(\lambda)Cx} d\lambda \tag{3.1}$$

where $f(\lambda)$ is the normalized emission spectrum of the dye. For solid materials, $\alpha(\lambda)$ C is the absorption coefficient of the material with units of cm^{-1}. In chemistry, the usage of molecular absorption cross section is common. The equations are the same, but care must be taken to insure correct units. Also, the equation is often expressed in base_{10}.

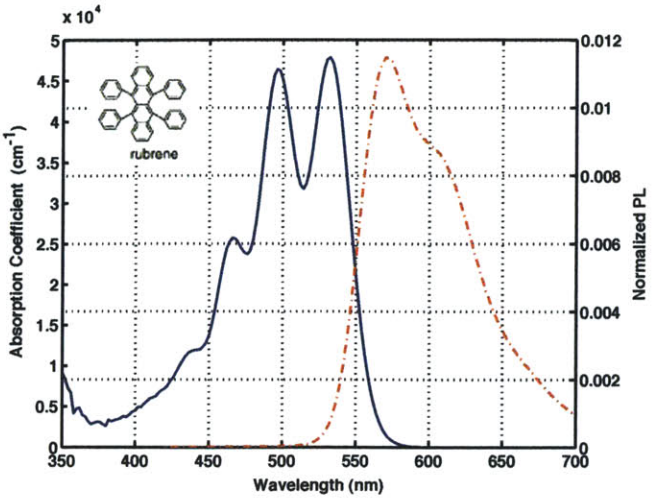

Figure 3-1: **Absorption and Photoluminescence Spectra for neat rubrene** – The absorption coefficient (solid) and photoluminescence spectra (dashed) are shown for a neat film of rubrene. The film was grown at a rate of 1.6 Å/s using a thermal evaporator. The peak absorption coefficient is 47,860 cm^{-1} at 532 nm.

The LSC results I will present in the experimental chapters are comprised of solid thin film layers evaporated onto the LSC substrate. Rather than the dye being uniformly dispersed throughout the substrate, it sits on one face. It is appropriate to use the absorption coefficient formalism where $\alpha(\lambda)$ is the absorption coefficient and C is the effective concentration of the thin film. For a film comprising 100% of a material, $C = 1$. Figure 3-1 shows the absorption coefficient and normalized photoluminescence spectrum for rubrene, a common dopant used in the OLED industry. The thin film was thermally evaporated at a rate of 1.6 Å/s using an custom evaporator manufactured by Angstrom Engineering. Absorption data and verified thickness were determined using an Aquila nkd8000 Spectral Reflectometer. The photoluminescence spectrum of the film was measured perpendicular to the film using an Acton Research Spectrasense detector and monochromator. A 408 nm laser with power of 3.7mW was used to excite the sample.. The peak absorption coefficient is 47,860 cm^{-1} at 532 nm.

To compute a useful path integral to estimate, r, we would like to compute the

Molecule Name	$1-r$			η_{trans}			Stoke's Shift (nm)
	12.5	25	50	12.5	25	50	
Alq_3	0.96	0.94	0.90	0.18	0.18	0.17	136
DCJTB	0.52	0.43	0.34	0.60	0.56	0.50	133
Rubrene	0.62	0.55	0.47	0.65	0.62	0.58	38
Imaginary	0.94	0.89	0.81	0.73	0.72	0.70	103

Table 3.1: **Self-absorption for common OLED materials**– This table shows the fractional intensity and η_{trans} values for notable OLED molecules. The quantum yield for Alq_3 is 25%, while the remaining materials have are assumed to have unity quantum yield.

average fractional intensity, i.e. $1-r$, arriving at the PV over all emitted angles. We make the following assumptions and approximations (1) PV is attached to four sides of the LSC. The path length from the center of the LSC approximates the average path length. (2) The thickness, t_{film} of the film is adjusted to achieve an optical density of 1 at the absorption peak. This guarantees that 90% of light at the peak wavelength is absorbed, i.e. η_{abs} is near unity. (3) Any ray emitted in the film is waveguided in the film and in the LSC substrate. As a result, the effective film concentration is $C = t_{film}/D$. Noticing that $x = L/2$ and $L/(4D) = G_{geo}$, the average fractional transmitted intensity, $1-r$, as a function of G_{geo} is:

$$[1-r](G_{geo}) = \frac{\int_{-\pi/4}^{\pi/4}\int_{\theta_{crit}}^{\pi/2}\int_{0}^{\infty}\sin(\theta)f(\lambda)\,e^{\frac{-2\alpha(\lambda)t_{film}G_{geo}}{\sin(\phi)\sin(\theta)}}\,d\lambda\,d\theta\,d\phi}{\cos(\theta_{crit})\frac{\pi}{2}} \tag{3.2}$$

Figure 3-3 shows the results of this calculation and the calculates η_{trans} for rubrene on a glass substrate, assuming η_{PL} is unity. As the geometric factor increases, the average path length increases. The fraction of light reaching the PV falls exponentially, but the effect on η_{trans} is not exponential due to the multiple generation events in the LSC.

The above calculation is repeated for two other common OLED materials Alq_3 and DCJTB. Their chemical names are, *tris* (8-hydroxyquinoline) aluminum and 4-(dicyanomethylene)-2-t-butyl-6(1,1,7,7-tetramethyljulolidyl-9-enyl)-4H-pyran, respectively. Alq_3 is an extremely common host material and DCJTB is a red dopant.

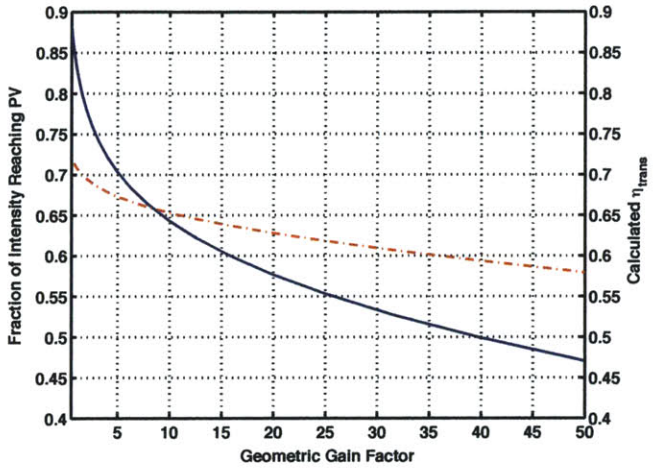

Figure 3-2: **Average Self-Absorption versus geometric gain** – Plotted is the fraction of light emitted from the center of an LSC that reaches an attached PV versus geometric gain (solid) and η_{trans} (dashed) assuming 100% quantum yield for a neat film of rubrene with OD1 in the vertical direction. The fraction of light falls exponentially, as predicted by Beer's Law, but η_{trans} falls sub-exponentially as a result of successive generations contributing to the total light reaching the PV.

Finally, a fourth imaginary molecule is calculated. It consists of the absorption spectrum of rubrene but the emission spectrum of DCJTB. This data is provided in Table 3.1. Alq_3 has the least self-absorption, however, η_{trans} is very low due to its quantum yield of 0.25. Rubrene and DCJTB have similar performance, but the imaginary combination of the two perform better. We will return to this possibility in the next chapter.

3.2 Two Dimensional Numeric LSC model

The previous section developed the weighted path length integral to calculate the amount of light reaching the PV. This calculation assumes that light emitted in the center of an LSC captures the characteristic behavior of the device. Perhaps light absorbed and re-emitted close the the PV edge will have a better collection efficiency, thereby boosting the overall light collection. This model needs to sum each $Q^{(i)}$ over all x and y until the model suitably converges.

The algorithm is straightforward, but computationally expensive. The problem scales with the resolution in the x-direction, y-direction and wavelength. To make the problem tractable we assume each emission generation is assumed to have the same spectra. The assumption is fair since the high energy wavelengths are the ones being heavily re-absorbed. This assumption is, also, conservative as it over-estimates self-absorption. With this assumption, the problem scales only in x and y.

The first step is the calculation of the fractional intensity matrix, $\boldsymbol{F_{trans}}$ for the amount of light reaching the attached PV's for all x and y. The integral is weighted by the distance to each attached PV. For instance, a point in the middle of the LSC will see similar paths to all attached PV, while a point near an LSC edge will see one PV closeby, one far away and two a middling distance away. Such a mapping is shown for a rubrene film with a geometric gain of 25 as discussed above in Figure 3-3. The excitation over all wavelength is integrated at each point and re-emitted via the emission matrix, $\boldsymbol{E^{(1)}}$. The light collected after the first generation is $\boldsymbol{T^{(1)}} = \boldsymbol{E^{(1)}F_{trans}}$.

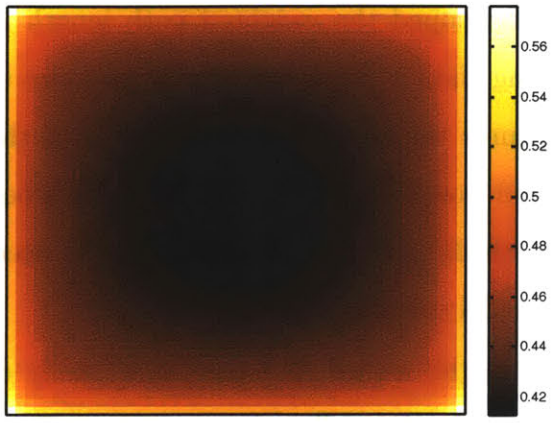

Figure 3-3: **2D Path Integral Map** – This map shows the two dimensional mapping of light to the attached PV for a rubrene LSC with geometric gain of 25. Light from the center of the LSC has the lowest coupling, while light near the edge couples most favorably. This mapping is applied with each successive generation to compute the total light coupled to the PV.

The second step is to generate a convolution kernel, $\boldsymbol{K}$ for the self-absorption in the film. Since every point emits isotropically, this convolution kernel is the same for every point. It calculates how much light is re-absorbed in each direction relative to itself. Then, $\boldsymbol{E}^{(2)} = \eta_{PL}\boldsymbol{K} * \boldsymbol{E}^{(1)}$. The convolution sum is carried out in as a multiplication in Fourier space for efficiency. The process repeats itself for each subsquent generation until the total light collected converges. Then η_{trans}, or Q, is the sum of the light collected for each generation divided by the initial excitation. For the rubrene case illustrated, η_{trans} is 0.64 compared to 0.62 as calculated by the self-absorption path integral in Equation 3.2.

Having determined that the self-absorption path length integral allows for a good approximation of η_{trans}, any dye or concentration of dyes can easily be analyzed knowing their absorption and emission spectra and quantum yield of photoluminescence. The full two-dimensional model can be left to situations, such as non-uniform excitation.

Chapter 4

Pathway to an Efficient LSC

4.1 Historical Implementations

The LSC concept was first introduced by Weber and Lambe in 1976.[12] This paper presented a complete two dimensional path integral to compute η_{trans}, and computes the limits for extremely high and extremely low self-absorption. The paper recommends the usage of rare earth doped materials, such as neodymium, and organic laser dyes.

Experiments with rare earth doped glass and rhodamine 6G followed shortly.[18] Weber and Levitt used *ad hoc* materials as their LSC's. The rhodamine LSC was cut from a drafting square, and the neodymium glass was used as purchased. In the case of the neodymium glass, η_{abs} was the largest factor limiting performance, while the rhodamine suffered large self-absorption losses. Of importance to this work, is the authors' suggestion to add material species that accept excitations and emit at longer wavelengths, such as the excitation transfer from rhodamine 6G to M-cresyl violet observed in solution. Rare earth experiments using uranyl-doped were, also, conducted.[19] The absorption strength was reported to be five orders of magnitude higher and neodymium glass, but overall performance suffered due to quantum yields near 30%.

In the late 1970's and early 1980's a systematic study of organic laser dyes for use in LSC's was conducted. [15][13] Batchelder, et al, tabulated self-absorption integrals

for eighteen common dyes. The best candidate dye was DCM (4-dicyanomethylene-2-methyl-6-(p(dimethylamino)styryl)-4H-pyran). DCM is commonly used in OLEDs and is a precursor to DCJTB. Typical efficiency measurements, determine flux gain arriving at the reference PV and extrapolate TPCE. All systems with geometric gains greater than 25 had efficiencies below 2%. Batchelder's largest concern was dye stability and photodegradation. For dyes dissolved in methanol, the half-lives ranged from 2000 to 10,000 hours, but in PMMA they decreased to 300 to 3000 hours. The measured bleaching rate for rhodamine-590 was 10^{-6} molecules/photon. Due to these measurements, serious concern shadowed the potential for an LSC that could compete with the robustness of inorganic systems.

Slightly prior to Batchelder's exhaustive work, the concept of multiple dye transfer was explored.[20] Since any single dye is not likely to cover the full solar spectrum, using multiple dyes obviously increases η_{abs}. If the dye concentrations are dilute, and no direct interaction exists between dyes, when higher energy dye emits light, the probability that it overlaps the absorption spectrum of a lower energy dye is great. When a lower energy dye absorbs the radiation of a higher energy dye, the process is called radiative energy transfer. Furthermore, each dye must have a high quantum yield for best performance. When the organic dye concentrations are high and the intermolecular spacing is small, interaction between molecules exists. Optical excitation energy can be transferred through dipole-dipole coupling of the two molecules. This process is also known as Förster resonance energy transfer (FRET). The rate of energy transfer between the higher energy donor and the lower energy acceptor is given by:[16]

$$K_{ET}(R) = \left(\frac{1}{\tau}\right)\left(\frac{R_0}{R}\right)^6 \tag{4.1}$$

where R_0 is the Förster radius and τ is the average donor lifetime in the absence of an acceptor molecule. When $R = R_0$, the donor molecule has an equal probability of photoluminescing itself or transferring its excitation to an acceptor molecule. The characteristic Förster radius is evaluated via the following integral:[16]

$$R_0^6 = 1.25x10^{17} \frac{\eta_{PL}}{n^4 c^3} \int F(\lambda)\alpha(\lambda)\lambda^2 d\lambda \tag{4.2}$$

where n is the index of refraction of the host, c is the speed of light, $f(\lambda)$ is the normalized emission spectrum of the donor and $\alpha(\lambda)$ is the molar extinction coefficient of the acceptor. In a multiple dye system with 100% FRET, all excitations are emitted by the lowest energy, or terminal dye. Now, the self-absorption behavior of only the final dye needs to be optimized. Swartz, et al, indicated partial FRET in their rhodamine-6G/coumarin-6 LSC based on observed emission spectra, but not quantified. They predicted onset of FRET at concentrations one order of magnitude higher than their working concentration, and their excitation wavelength directly excited both species. Nevertheless, the principle is sound.

4.2 Material Stability Improvements

After a period of disinterest, the synthesis of stable, highly efficient perylene dyes reinvigorated LSC work.[21] BASF sells perylene dyes across the visible spectrum that have quantum yields above 90%. Recently, results of LSC's with geometric gains of 10 and 20 consisting of a custom perylene dye were reported.[22]. At the absorption peak of the perylene dye, the EQE was 28% and 22% for LSC's of geometric gain 10 and 20, resulting in $\eta_{TPCE}$of 1.6% and 1.1%, respectively, measured under a calibrated solar simulator. This work is fairly unique in that it measures the EQE over wavelength and power via the attached PV cell. Additional perylene was used as the LSC dye material in work investigating the use of photonic bandstop filters to increase η_{trap}.[23] I will mention this work in the concluding remarks of this thesis.

Another possible candidate for the dye in an LSC is the inorganic quantum dot. Being crystalline in nature, it has been argued they would make stabler alternatives to organics.[24] A QD's bandgap is a function of the dot size. This feature allows tailoring of the QD's to achieve full spectrum coverage. At the present time, efficiency is limited by the low quantum yield of the dots.

Finally, OLED technology is driving the lifetime of organic materials. Univer-

sal Display Corporation advertises phosphorescent OLED materials with operational lifetime exceeding 300,000 hours. Alq_3 is the predominant host organic in current production OLEDs.

4.3 Strategy to Minimize Self-absorption

Principally, the use of FRET is a method to increase the amount solar spectrum that is absorbed, η_{abs}, without incurring extra self-absorption of the high energy dyes.[25] A second benefit is a looser constraint of η_{PL} for higher energy dyes. The lower η_{PL} can be made up by closer intermolecular spacing. However, FRET does not necessarily increase η_{trans}. For instance, if the acceptor dye has a large overlap integral, the added benefit of absorbing more light is outweighed by the increased self-absorption. Also, if the final dye has a low η_{PL}, it will be a photon trap. Because all the excitations are funneled to the final dye, this dye must have excellent quantum yields and low self-absorption. For the terminal dye, a delicate balance must be struck. If the concentration is high, energy transfer is most likely, but self-absorption will be greatest. If the concentration is low, self-absorption will be low, but transfer may be incomplete. In general, the terminal dye should be in just a high enough concentration to fully accept all donor excitations. For a matrix of molecules, this means at least one terminal acceptor should be found within a Förster radius of each donor. Any extra acceptor within this radius only slightly increases the transfer rate, since it scales $(\frac{R_0}{R})^6$, but doubles the self-absorption probability .

The phycobilisome antenna found in cyanobacteria is a system that meets these requirements. The phycobilsome is a highly structured complex consisting of multiple chromophores and interconnecting protein that harvests sunlight.[26] The three major chromophores are phycoerythrin (PE), phycocyanin (PC) and allophycocyanin (AP). A model of the complex and its absorption and emission spectra are shown in Figure 4-1. The PE chromophores sit on the exterior of the rod-like appendages and do the bulk of sunlight harvesting. They transfer their excitation to the PC chromophores through Förster energy transfer, who in turn transfer the excitation to the AP chro-

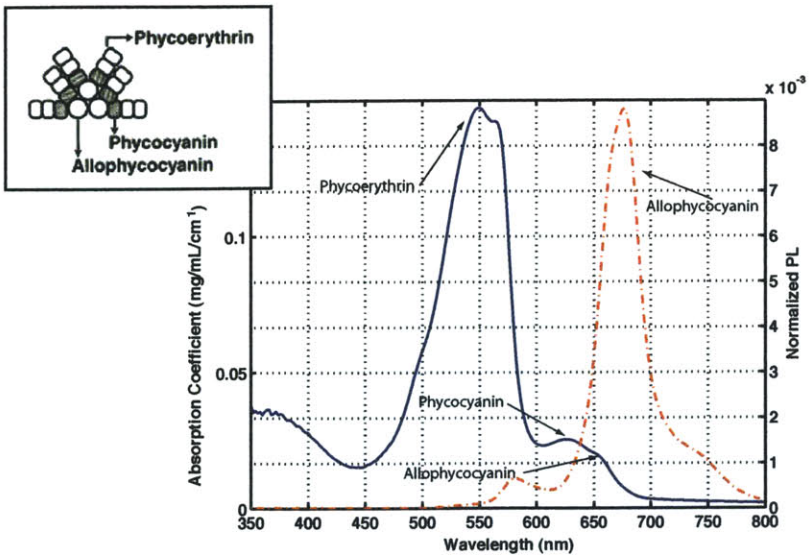

Figure 4-1: **Phycobilisome structure and Spectra** – The absorption coefficient (solid) and photoluminescence spectra (dashed) of the phycobilisome antenna in phosphate buffer pH 8.0 is shown. The PE chromophore has the largest absorption coefficient at 565 nm. It successfully transfers it excitation to the AP chromophore that is responsible for all the emission.

mophores in the core of the complex. Typically, the AP chromophore then transfers its excitation to a photosynthesis complex, but in its absence, it photoluminesces. All of the emission is from the AP chromophores. The ratio of PE to AP is greater than 3:1. Here we have the energy funneling from a greater number of high energy dyes to a smaller number of low energy dyes.

In terms of an LSC dye, the PE chromophore effectively extends its Stoke's shift by transferring its energy to the AP chromophore. Similar to this approach, the concepts of energy transfer can be used to design the imaginary dye mentioned in chapter 3. The imaginary dye has the absorption properties of rubrene, but the luminescence properties of DCJTB. The imaginary dye has a larger Stoke's shift than the rubrene dye and a higher η_{trans} than either dye. The result is a more efficient LSC. Along the way Alq_3 is added to the device to maximize η_{abs}. The fabrication and testing of this LSC is presented in the next Chapter.

The application of Förster energy transfer is commonplace in OLED devices. Be-

cause many dyes have poor electrical performance, they are doped into a host in thin regions, known as emissive regions. Electrons and holes are driven to the emissive region with an electric field where they tend to generate excitations, or excitons, on the dye molecules. Alq_3 is a common host that is chemically compatible with a number of dyes. Alq_3 is often paired with DCM to create a red OLED. The Förster radius was calculated to be 3.3 nm and complete transfer was determined at an intermolecular spacing of 2.4 nm.[27][28] Since DCJTB, is closely related to DCM, we expect efficient transfer, as well. In fact, an Alq_3:DCJTB OLED using rubrene as a transfer mediator has been developed.[29] With their compatibility in OLED's known, the combination must be optimized for an LSC.

Chapter 5

LSC Fabrication and Testing

5.1 LSC Fabrication

The optimized LSC combines three main components: (1) substrate, (2) attached PV and (3) optimized thin film. The design and fabrication of each is described in subsections.

5.1.1 Optimized Thin Film

All thin films are evaporated using a thermal evaporator, manufactured by Angstrom Engineering, with a base pressure below 10^{-6} torr. Deposition is controlled through Sigma Instruments SQS-242 control software. The system has six evaporation sources and permits co-evaporation of up to three materials using four crystal head monitors. Three of the monitors are located close to the evaporation source and the final sensor is located next to the target. This provides for precise control of host and dopant rates. The evaporator is enclosed in a glove box kept under high purity nitrogen to limit oxygen and water contamination.

The focus of optimization is on the terminal dye, DCJTB. The goal is to minimize its concentration in the final LSC film while achieving complete transfer from the donor dyes. As expected from OLED literature, Alq_3 transfers completely to DCJTB at low concentrations. Figure 5-1 shows the photoluminescence of a series

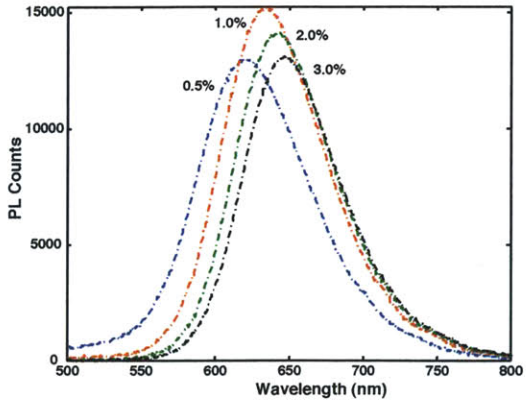

Figure 5-1: **PL Spectra of Alq_3:DCJTB(x%)** – The PL spectra of Alq_3:DCJTB(x%) is plotted for concentrations between 0.5% to 3.0%. The thickness of Alq_3 was maintained at 50 nm. Optimal transfer occurs at Alq_3:DCJTB(1%), with an estimated η_{PL} between 0.85-0.95 compared to a reference sample of the same thickness with no DCJTB present. η_{PL} drops off 8% and 18% at concentrations of 2% and 3% due to concentration quenching.

of Alq_3:DCJTB(x%) thin films excited with a 408 nm laser. All concentrations are specified in volume percentages. The thickness of the Alq_3 portion of the device was maintained at 50 nm. The measurement was taken perpendicular to the thin film, thereby minimizing red shift in the spectrum due to re-absorption. In general, all PL spectra are taken perpendicular to a film of minimal thickness. At 0.5% only a small contribution of the Alq_3 PL spectrum is observed. To judge energy transfer from spectra, both magnitude and shape must be taken into account. In this case, η_{PL} of Alq_3 is much less than that of DCJTB. When energy transfer takes place, it should be accompanied by a large increase in total counts. If only spectrum shift is observed, either severe concentration quenching is present or self-absorption. Optimal transfer occurs at Alq_3:DCJTB(1%), with an estimated η_{PL} between 0.85-0.95 compared to a reference sample of the same thickness with no DCJTB present.

The optimization for energy transfer between rubrene and DCJTB is trickier. Rubrene, also concentration quenches, and as a consequence, the Förster radius for energy transfer gets smaller as the concentration of rubrene increases. If DCJTB did

not concentration quench we could alleviate this problem by increasing the DCJTB concentration. Unfortunately, it does and we need to trade the benefits. Figure 5-2 shows the PL spectra for Alq_3:Rubrene(40%):DCJTB(x%). The excitation is a 532 nm laser source. At this excitation wavelength, only the rubrene component of the film is excited. Here, the optimal DCJTB doping concentration is 3% versus 1% for the Alq_3 only film. The interesting features occur in the 1% spectra. Here, there is evidence of the rubrene PL peak at 575 nm and the rubrene PL shoulder at 615 nm (see Figure 3-1) but they have changed magnitudes. It appears that the higher energy portion of the spectra is being transfered to DCJTB preferentially than the lower energy portion of the spectra. A final note is that the peak location for 3% doping is blue-shifted from the peak location for 3% doping in the Alq_3 only film. Perhaps rubrene is buffering DCJTB's predilection to concentration quench.

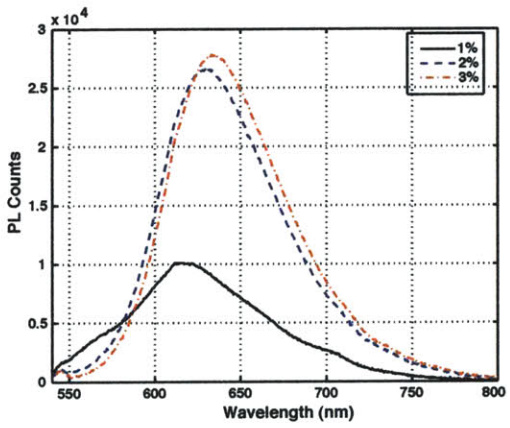

Figure 5-2: **PL Spectra of Alq_3:Rubrene(40%):DCJTB(x%)** – The PL Spectra of Alq_3:Rubrene(40%):DCJTB(x%) is plotted for concentrations between 1.0% to 3.0%. The excitation is a 532 nm laser source. The optimal doping concentration of DCJTB is 3%. The interesting features occur in the 1% spectra. Here, there is evidence of the rubrene PL peak at 575 nm and the rubrene PL shoulder at 615 nm (see Figure 3-1) but they have changed magnitudes. It appears that the higher energy portion of the spectra is being transfered to DCJTB preferentially than the lower energy portion of the spectra.

For completeness, the same set of films were excited at 408 nm, where only the

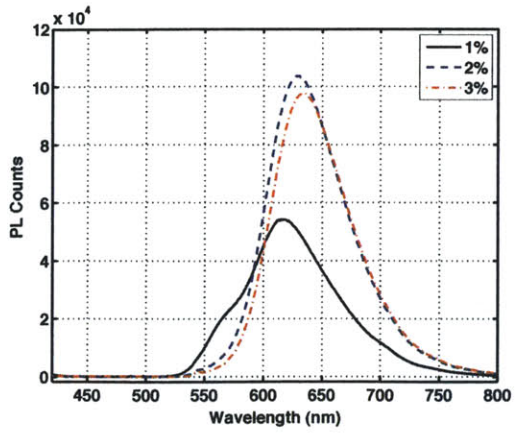

Figure 5-3: **PL Spectra of Alq_3:Rubrene(40%):DCJTB(x%)** – The PL Spectra of Alq_3:Rubrene(40%):DCJTB(x%) is plotted for concentrations between 1.0% to 3.0%. Now, the excitation is a 408 nm laser source. The optimal doping concentration of DCJTB is 2%. At low DCJTB doping concentrations, Alq_3 transfers to both rubrene and DCJTB.

Alq_3 molecules absorb. At low concentrations of DCJTB, excitation is transferred to both rubrene and DCJTB. And again the high energy portion of the rubrene spectrum is transferring preferentially to the DCJTB. At higher concentrations, it is unclear if the excitations are transferring directly to DCJTB or if they are being mediated by the presence of rubrene. To optimize both donors, a DCJTB concentration of 2% is chosen.

5.1.2 Choice of Substrate

In this LSC, the dye molecules are evaporated onto the substrate forming a thin film. As such the η_{trap} is determined by the index of refraction of the film, not the substrate. There is now an interface between the film and the substrate that must be taken into consideration. If the substrate's index of refraction is less than the film's, some waveguiding will take place in the film. Light travelling in the film will be self-absorbed within microns.

Using the Aquila nkd8000 spectral reflectometer, the transmission and reflection

of the optimal thin film was taken. The index of refraction was determined via a Cauchy model fit in the transparent wavelength region of the film. The index gently falls from 1.72 to 1.68 over the region where DCJTB emits. To match the index, SF10 lead oxide glass from Schott was selected. At 632 nm, the index of refraction is 1.72 and the internal transmittance was 0.99 over 25 mm. This glass is index matched and highly transparent at the emission wavelengths. The overall dimensions of the glass are 100 mm x 100 mm x 1mm. Attaching PV to all sides gives a geometric gain of 25.

5.1.3 Choice of Photovoltaic

The prime consideration for a photovoltaic is its EQE. Recalling equation 2.16, η_{PV} directly impacts the EQE of the LSC. Commercially available PV was not developed for usage in an LSC. Nonetheless, multi-crystalline (Evergreen Solar) and back-contact single crystalline (Sunpower) were evaluated. The multi-crystalline was diced to into thin strips 3 mm wide, and the single crystalline was diced into strips 8 mm wide. Dicing a solar cell in this way creates unpassivated surfaces that could be recombination centers. For single crystalline cells, this is a worry since it relies on extremely long diffusion lengths for its efficiency. The EQE's of thin strips of these PV are plotted in Figure 5-4 after they have been diced into strips. The excitation spot size was 2mm x 1mm centered in the strip and taken at numerous locations along the length. The wavelength of excitation was selected with a monochromator and chopped at 90 Hz. The short circuit current of the PV was sensed with a lock-in amplifier and ratio-ed the to the output of a calibrated Newport 818-UV photodiode. The single crystalline cell has a flat response across the whole spectrum with an EQE of 0.87 at the peak DCJTB emission wavelength.

From equation (2.4), η_{TPCE} of the LSC depends on the V_{oc} and FF of the PV. V_{oc} is intensity dependent and should improve with increased photocurrent due to concentration. The FF, on the other hand, degrades if there is appreciable series resistance in the PV strip. At full sun illumination, multi-crystalline strips were found to be unacceptable. The series losses severely diminished the FF. This was not

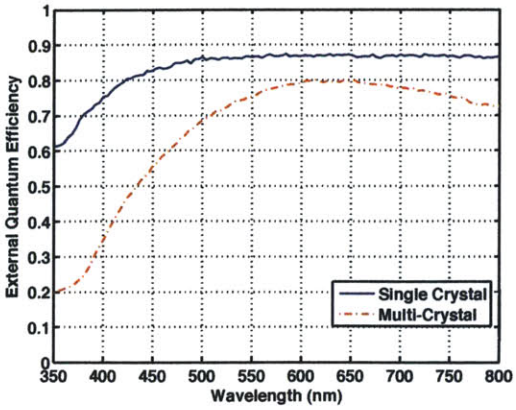

Figure 5-4: **EQE spectrum of single and multi crystalline solar cells** – Plotted are the EQE spectrum of single crystal and multi-crystal PV strips just prior to incorporation into a LSC. The single crystal has better response across the whole spectrum. At the emission peak of DCJTB, the EQE's are 0.87 and 0.8 for respective cells.

the case for back-contacted crystalline cells. This reinforces the need for a PV strictly designed for usage in an LSC.

For these reasons, the back-contact single crystalline cell was selected. Once the PV is constructed into a LSC, the EQE of the PV may change because anti-reflection coatings and optical structures are designed for normal illumination.

5.1.4 Fabrication Steps of Optimized LSC

The details of assembly are as follows:

1. Using a dicing saw, the cell was cut into 8 mm strips. The kerf followed the SiO_2 line between contact fingers.

2. One strand of 18 gauge wire was soldered (2% Ag content) to the anode and cathode of the cell strip.

3. Due to the fragility of the cell strip, a rigid support of 1/2" acrylic was machined. In one step, the strip was epoxied to the acrylic support and the glass was

epoxied normal to the plane of the strip. Curing took place overnight to alleviate thermal expansion mismatch inherent in curing at temperature. The epoxy was optical grade Epotek - 301.

4. The assembled LSC without film was passed into the evaporator glove box and mounted to sample plate inside the evaporator. Alq_3, rubrene and DCJTB were loaded into separate evaporation sources. Baffles were placed between evaporation sources to prevent cross-talk at the crystal monitors. Using volumetric tooling factors determined previously, rate were adjusted to grow a 500 nm Alq_3:Rubrene(45%):DCJTB(2%) thin film.

The final LSC has PV attached to only a single side. The other three sides are blackened to prevent reflections. Due to the symmetry of the device, any excitation that maintains the symmetry of the LSC can be multiplied by a factor of four to account for cells that could be attached to all edges. Any measurement that uses this factor must be reported with a geometric gain of 25, although the LSC as constructed has a geometric gain of 100. The film thickness is optimized to absorb 95% of the light using a two pass geometry provided by means of a silver mirror placed below the LSC. The actual absorption will be reduced because of the reflection off the high index glass. The use of the two pass geometry allows for a lower effective film concentration that will improve η_{trans}.

5.1.5 Measured Absorption Constants and EQE Measurement

With the complete LSC constructed, the absorption and photoluminescence spectrum of the film are measured. To avoid deterioration of the LSC film, a microscope slide which sat adjacent to the LSC in the evaporator is used. Figure 5-5 shows the final spectra of the optimal film. Indeed, the optimal film has the properties of the imaginary film proposed in Chapter 3, with extra absorption contributions from Alq_3. The average transmission path integral for this film with geometric gain of 25 is: $1 - r = 0.62$. This value of $1 - r$ is greater than the calculated value for rubrene

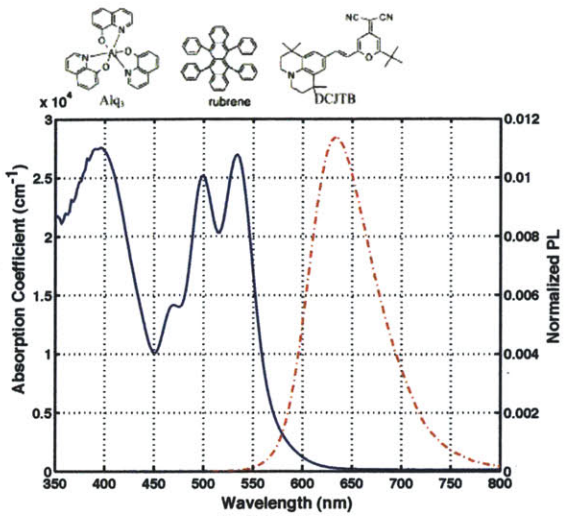

Figure 5-5: **Absorption and PL spectrum of Alq$_3$:Rubrene(45%):DCJTB(2%)** – Plotted are absorption coefficient (solid) and photoluminescence spectrum (dashed) of Alq$_3$:Rubrene(45%):DCJTB(2.5%). Compared to Figure 3-1, the overlap is greatly reduced. Computation of the $1 - r$ path integral for the 500 nm film gives 0.617

and DCJTB, but less than the imaginary system. *Alas, we have improved upon self-absorption by incorporating energy transfer!* Assuming the film has η_{PL} of 0.90, and using η_{trap} for the high index glass, η_{trans} is calculated at 0.62. We have everything we need to model the EQE of the system.

The EQE of the LSC is measured using the same set-up explained previously. We maintain symmetry by illuminating in the middle of the device and multiplying by four. Figure 5-6 shows the results of this measurement and the predicted value. At the EQE maximum, 32% of the photons impinging on the device become charge in the external circuit. With the geometric gain of 25, this corresponds to an eight times increase in photocurrent for light of that wavelength.

The final test of an optimized test is the measurement of η_{TPCE} via a solar simulator. This work was limited to a solar simulator producing a 2" x 2" beam of AM 1.5 Global Light at 8950 W/m^2, equivalent to 9 suns. As has been developed throughout this thesis, illumination of the center of device approximates total device performance. All but the center square inch of the LSC was masked and the LSC

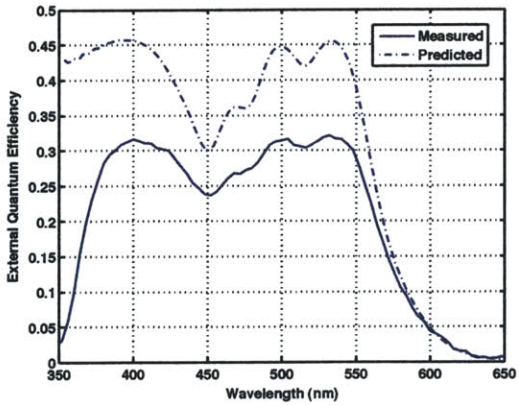

Figure 5-6: **Optimized LSC External Quantum Efficiency** – This plot shows the measured EQE of the optimized LSC design and the predictions for the model developed in this thesis. Overall, 32% of the photons impinging on the device become charge in the external circuit. This value is $\frac{2}{3}$ of the predicted value, which testifies to the quality of the LSC construction.

illuminated. The high simulator intensity is meant achieve a similar photocurrent that the whole unmasked LSC would see under 1 sun conditions. This will preserve the proper V_{oc} and FF. The table 5-1 summarizes the results. As a check, equation 2.3 was applied to the measured EQE using the AM 1.5 Global spectrum at 9 suns. The expected short circuit current density was 7.5 mA/cm^2 for one edge. This agrees with the measured value to within 5%.

	Incident Power (mW/cm^2)	J_{sc} (mA/cm^2)	V_{oc} (V)	P_{max} (mW/cm^2)	FF	η_{TPCE}
PV (1edge)	0.895	7.90	0.61	3.64	0.76	0.0041
PV (4 edges)	0.895	31.6	0.61	14.56	0.76	0.0164

Table 5.1: η_{TPCE} **for optimized LSC**– This table summarizes the output of the LSC measured via the attached PV under 9 suns illumination of AM 1.5 global spectrum. The center 1 square inch of the LSC was illuminated. The calculated η_{TPCE} for a four-sided LSC of geometric gain of 25 is 1.64%.

Chapter 6

Conclusion

This thesis broke the subject of the LSC into two parts, theoretical modeling and experimentation. The models for LSC performance were reviewed and the basic determinants of performance were distilled. Two different models were developed to demonstrate the coupling of photoluminescence efficiency, waveguide trapping and self-absorption. These three factors contribute to the bulk parameter, η_{trans}. The remaining parameters needed to determine external quantum efficiency are the efficiency light absorption, η_{abs}, and the EQE of the attached PV, η_{PV}. A simple path integral has been shown to capture the physics of self-absorption rather than relying on a computationally expensive numerical model. The performance of a system of compatible dyes in an LSC can be determined if their absorption and emission spectra and total quantum yield are known.

Experimentally, this work presents a number of firsts. For the first time, thermally evaporated small molecule organics have been used. For the first time, a higher η_{trap} has been achieved by emitting light in a high index medium. For the first time, solar cells were diced to approximate the dimension of the LSC edge. Because of this, multi-crystalline solar cells were deemed unsuitable. Most importantly, this is the first time energy transfer was used to optimize self-absorption of the terminal dye.

Apart from these firsts, the LSC performed extremely well. The total power conversion efficiency was 1.6% for an LSC with geometric gain of 25. A peak EQE of 32% was observed at the absorption peak of both dyes in the film– Alq_3 at 408 nm

and rubrene at 532 nm. This is the highest EQE the author has seen in the literature!

The techniques set forth in this thesis should form the basis of how to incorporate additional dyes, organics, quantum dots, or other, into the LSC to capture the full solar spectrum. Simply making extra plates and separating the dyes will suffer from low geometric gains. Energy transfer needs to be engineered into LSC design. This requires control of molecule spacing at the nanometer level. This work uses the approach of doped thin-films, while the phycobilisome model from nature uses chemically bonded complexes. Synthetic chromophore dendrimers have the promise of approximating a chemically bound system.

Finally, this work did not address the optical design of the substrate. A simple air interface was relied upon for waveguideing. Omni-directional dielectric mirrors can provide a 25% improvement. And, simply adding an anti-reflective layer can improve performance devices by 10%.

In the near future, the development of highly efficient near-infrared dyes is critical to the progress of the LSC. When a suitable candidate surfaces, the LSC will achieve results foreshadowed in Figure 2-2. The author firmly believes a 12-15% efficient LSC with geometric gains over 100 is on the horizon.

Bibliography

[1] J. Goldemberg and T. Johansson. World energy assessment update. Technical report, United Nations Development Programme, 2004.

[2] Kaya Y. Impact of carbon dioxide emission control on gnp growth: Interpretation of proposed scenarios. *IPCC Response Strategies Working Group Memorandum*, 1989.

[3] Hoffert M.I., Caldeira K., Jain A.K., Haites E.F., Harvey L.L.D., Potter S.D., Schlesinger M.E., Schneider S.H., Watts R.G., Wigley T.M.L., and Wuebbles D.J. Energy implications of future stabilization of atmospheric co2 content. *Nature*, 395(29):882–884, October 1998.

[4] Green M.A., Emery K., King D.L., Hishikawa Y., and Warta W. Solar cell efficiency tables (version 29). *Progress in Photovoltaics Research and Applications*, 15:35–40, 2007.

[5] Green M.A. Silicon photovoltaic modules: a brief history of the first fifty years. *Progress in Photovoltaics Research and Applications*, 13:447–455, 2005.

[6] Zhao J., Wanh A., and Green M.A. 24.5efficiency perl cells on fz substrates. *Progress in Photovoltaics Research and Applications*, 7(471-474), 1999.

[7] Schemla M. and www.photon magazine.com. Market survey on cell and module production 2006, March 2007.

[8] http://www.solarbuzz.com/Moduleprices.htm. Solar module price highlights, May 2007.

[9] Sariciftci N.S. and Hoppe H. Organic solar cells: An overview. *Journal of Materials Research*, 19(7):1924–1945, 2004.

[10] J. Xue, S. Uchida, B.P. Rand, and S.R. Forrest. Asymmetric tandem organic photovoltaic cells with hybrid planar-mixed molecular heterojunctions. *Applied Physics Letters*, 85(23):5757–5759, 2004.

[11] Baldo M.A., Thompson M.E., and Forrest S.R. High-efficiency fluorescent organic light-emitting devices using a phosphorescent sensitizer. *Nature*, 403(6771):750–753, 2000.

[12] W.H. Weber and J. Lambe. Luminescent greenhouse collector for solar radiation. *Applied Optics*, 15:2299–2300, 1976.

[13] Batchelder J.S., Zewail A.H., and Cole T. Luminescent solar concentrators. 2: Experimental and theoretical analysis of their possible efficiencies. *Applied Optics*, 20(21):3733–3754, 1981.

[14] Earp A.A, Smith G.B., Franklin J., and Swift P. Optimization of a three color luminscent solar concentrator daylighting system. *Solar Energy Materials and Solar Cells*, pages 411–426, 2004.

[15] Batchelder J.S., Zewail A.H., and Cole T. Luminescent solar concentrators. 1: Theory of operation and techniques for performance evaluation. *Applied Optics*, 18(18):3090–3110, 1981.

[16] Pope M. and Swenberg C.E. *Electronic Processes in Organic Crystals and Polymers*. Oxford University Press, 1982.

[17] Madigan C.F. and Bulovic V. Solid state solvation in amorphous organic thin films. *Physicla Review Letters*, 91(24):Art. No. 247403, 2003.

[18] Levitt J.A. and Weber W.H. Materials for luminescent greenhouse solar collectors. *Applied Optics*, 16(10):2684–2689, 1977.

[19] Reisfeld R. and Neuman S. Planar solar energy converter and concentrator based on uranyl-doped glass. *Nature*, 274:144–145, 1978.

[20] Swartz B.A., Cole T., and Zewail A.H. Photon trapping and energy transfer in multiple-dye plastic matrices: an efficient solar energy concentrator. *Optics Letters*, 1:73–75, 1977.

[21] Seybold G. and Wagenblast G. New perylene and violanthrone dyestuffs for fluorescent collectors. *Dyes and Pigments*, 11(44):303–317, 1989.

[22] Slooff L., Kinderman R., Burgers A., van Roosmalen J., Buchtemann A., Danz R., Schleusener M., Chatten A.J., Farrell D., and Barnham K.W.J. The luminescent concentrator: a bright idea for spectrum conversion. In *20th European Photovoltaic Solar Energy Conference and Exhibition*, 2005.

[23] Glaeser G.C. and Rau U. Collection and conversion properties of photovoltaic fluourescent collectors with photonic band stop filters. In Photonics for Solar Energy Systems. Andreas Gombert, editor, *Proc. of SPIE Vol. 6197*, 2006.

[24] Chatten A.J., Barnham K.W.J., Buxton B.F., Ekins-Daukes N.J., and Malik M.A. Quantum dot solar concentrators. *Semiconductors*, 38(8):909–917, 2004.

[25] Bailey S.T., Lokey G.E., Hanes M.S., Shearer J.D.M., McLafferty J.B., Beaumont G.T., Baseler T.T., Layhue J.M., Broussrd D.R., Zhang Y.Z., and Wittmershaus B.P. Optimized excitation energy transfer in a three-dye luminescent solar concentrator. *Solar Energy Materials and Solar Cells*, 91(1):67–75, 2007.

[26] MacColl R. Cyanobacterial phycobilisomes. *Journal of Structural Biology*, 124:311–334, 1998.

[27] Shoustikov A.A., You Y., and Thompson M.E. Electroluminescence color tuning by dye doping in organic light-emitting diodes. *IEEE Journal of Selected Topics in Quantum Electronics*, 4(1):3–13, 1998.

[28] Zhong G.Y., He J., Zhang T., Xu Z., Xiong Z.H., Shi H.Z, and Ding X.M. In situ photoluminescence investigation of doped alq. *Applied Physics Letters*, 80(25):4846–4848, 2002.

[29] Liu T.H., Iou C.Y., Wen S.W., and Chen C.H. Dcjtb doped red emitters in organic light-emitting devices. *Thin Solid Films*, 441:223–227, 2003.